AIIM

Association for Information and Image Management

1100 Wayne Avenue, Suite 1100
Silver Spring, Maryland 20910

301/587-8202

Centimeter

Inches

MANUFACTURED TO AIIM STANDARDS
BY APPLIED IMAGE, INC.

1 of 1

CONF-9309170--2

BNL-60341

Target Design Considerations for High Specific Activity $[^{11}C]O_2$

Richard A. Ferrieri*, David L. Alexoff, David J. Schlyer,
Keith McDonald and Alfred P. Wolf

Brookhaven National Laboratory, Department of Chemistry
Upton, New York, U.S.A. 11973

INTRODUCTION

The importance of receptor imaging has stressed the need for pharmacologically active compounds that are labeled with high specific activity carbon-11. $[^{11}C]H_3I$ is the most versatile, and by far the most widely used precursor for labelling such compounds with carbon-11 through $[^{11}C]$-methylation (Langstrom, *et al.*, 1976; Burns, *et al.*, 1984; Suzuki, *et al.*, 1985; Farde, *et al.*, 1986; Watkins, *et al.*, 1988; Hatano, *et al.*, 1989; Pascali, *et al.*, 1990; Dewey, *et al.*, 1990; Iwata, *et al.*, 1991). With careful handling of reagents for the reduction of $[^{11}C]O_2$ to $[^{11}C]H_3OH$, and for the subsequent iodination of $[^{11}C]H_3OH$ to $[^{11}C]H_3I$, we have found as little as 3 nmol of carrier carbon introduced at this stage of synthesis with the exclusion of the $[^{11}C]O_2$ target system contributions. However, in the routine preparation of compounds through N-$[^{11}C]$-methylation using $[^{11}C]H_3I$, total masses are always higher than the synthesis mass contribution. This suggests that the $[^{11}C]O_2$ target system contributes carrier carbon to the final product mass. This conclusion prompted our recent evaluation of target materials and target design for $[^{11}C]O_2$ production.

STUDIES IN TARGET MEASUREMENT OF CO_2 MASS

DESCRIPTION OF ANALYTICAL SYSTEM: As shown in Figure 1, the flame ionization detector (FID) from a Hewlett Packard 5890A Gas Chromatograph was modified for carbon oxide analysis by incorporating a miniature nickel catalyst methanizer into its jet and operating the detector at 400°C (Goekeler, 1989). The catalyst reduces CO and CO_2 to CH_4 (a detectable species by FID) prior to their entering the flame region of the detector. The catalyst operates efficiently using the same H_2 supply as that needed to sustain the flame, and exhibits remarkable stability in its day-to-day usage when maintained under a continuous helium stream at about 200°C. The detector also exhibits a linear response to CO_2 with over three orders of magnitude change in concentration thus simplifying instrument calibration, and is capable of handling large sample throughput which is convenient for operation with a packed chromatography column.

MASTER

DISTRIBUTION OF THIS DOCUMENT IS UNLIMITED

The modified FID can detect 10 ppb of CO_2 within a 4 mL volume sample of target gas at STP. This level of sensitivity is about 10^3 times higher than that seen with thermal conductivity detectors (TCD). Therefore, no preconcentration of samples is required, and a single 500 mL volume bulb of collected gas offers adequate sample for numerous measurements to be made. Typical methods of analysis using TCD required cryotrapping of CO_2 from large volumes of gas.

In the system shown in Figure 2, we used a 12 ft x 1/8 in. Porapak Q column with a 3:1 splitter at the column outlet to allow for on-line radioactivity measurements using a NaI scintillation detector. The system also has a small vacuum manifold which allows us to remove air once the sampling bulb is connected to the instrument. A 2-way switching valve allows us to sequentially fill and inject gas samples of known volumn and pressure.

RESULTS AND DISCUSSION: The analytical system previously described was used to measure CO_2 and total carbon concentrations within the UHP N_2 (99.999% purity, Matheson Gas Co.) used for producing $[^{11}C]O_2$. CO_2 concentrations as low as 2 pmol/cm^3 or 0.05 ppm were found. Total carbon concentrations were determined as CO_2 after combustion over CuO at 850°C, and were found to be 24 pmol/cm^3 or about 0.6 ppm. Our standard $[^{11}C]O_2$ production target is constructed of an aluminum alloy (approximately 97% purity), and has a volume of 212 cm^3 (3 cm i.d. x 30 cm length). The 16.5 miL thick front target window is also made from the same alloy. When pressurized to 10 atmospheres, the gas contribution amounts to 50 nmol of carrier carbon, assuming all carbon is combusted to CO_2 under irradiation conditions. However, levels of CO_2 arising from this target were much higher than this subsequent to irradiation from 17 MeV H^+ (13.4 MeV on gas) of varied intensity. In addition, the amount of CO_2 released was dose-rate dependent suggesting a material source of carrier carbon. Replacement of all organic seals (ie. front window o-ring and gas fittings) with indium gaskets failed to show an improvement in target performance suggesting that the aluminum itself was the source.

SURFACE ANALYSIS STUDIES USINGELECTRON INDUCED DESORPTION (EID) SPECTROSCOPY

DESCRIPTION OF ANALYTICAL SYSTEM: Electron probes are a commonly used analytical tool in material and surface analysis (Czanderna, 1975) because of their ease of generation at controlled energy and density. Electron probing of a surface can result in the emission of four types of particles (electrons, photons, ions and neutrals).

Information derived from the nature and states of one or more of these species can then be related back to the composition and morphology of the surface.

Electrons can undergo inelastic collisions with atoms or molecules on a surface raising them to various excited and/or ionized states thus causing desorption. Since the mass ratio of electrons to atoms is very small, kinetic energy exchanges are minimal. Electronic transitions, however, have a fairly high cross-section at modest electron energies (less than 100 eV), and therefore can be utilized to desorb the outermost monolayer of material adsorbed on a surface. Of course, kinetic energy exchange can become important with the impact of higher energy electrons thus allowing one to probe fairly deep into the bulk of the material.

The EID instrument, shown in Figure 3, is designed for high-energy electron impact to probe both surface morphology, and bulk material composition in target aluminum alloys. The system is comprised of a high vacuum chamber possessing an easy access port for sample introduction, a high energy electron source and electron containment cage, and a quadrupole mass spectrometer with electron induced ionization and electron multipler detector. Only emitted neutral species are monitored by the mass spectrometry, because surface emitted positive ions are accelerated out of the detection path of the spectrometer, and trapped by the electron containment cage.

RESULTS AND DISCUSSION: As seen in Figure 4, two bulk-bound states of carbonaceous material are observed in the aluminum alloy (6061) used as target material. These states were detected in our instrument as CO (m/z 28) and CO_2 (m/z 44), although only the CO_2 spectrum is shown here, from peaks appearing at 50 and 150 seconds into the EID scan. Upon deposition onto the surface of an oxide coating of approximately 10^4 monolayers thick, and upon exposure of that modified surface to 1 atmosphere of N_2 gas containing 10 ppm levels of CO_2, we observed a drastic change in the EID spectrum. Two new peaks are introduced by this treatment, appearing at 20 and 30 seconds into the scan. The short appearance times of these peaks lead us to suspect that they represent loosely bound surface carbon.

Results from our EID studies suggest that aluminum purity is perhaps not as important a criteria in target design for high specific activity $[^{11}C]O_2$ as the amount of material exposed to the beam, and/or the gas plasma during irradiation, since all aluminum surfaces will oxidize to some degree with time and exposure. This build-up in oxide will create a spongy overlayer on the surface which can act as an efficient sink for removal of carbonaceous material from the target gas. Of course, this process will be amplified if the target is frequently opened to air. Accumulated carbon can

then released back into the target gas during proton bombardment, by one or more mechanisms not yet understood. The levels of release should be contingent upon the irradiation conditions, and the degree of carbon saturation of the oxide.

STUDIES CORRELATING TARGET SURFACE AREA WITH TARGET MASS

EXPERIMENTAL PROCEDURE: We investigated the correlation between exposed surface and carrier mass generation by inserting aluminum alloy plugs of various lengths into a 212 cm^3 volume cylindrical target. Beam penetration in the unmodified target was calculated to be 27 cm assuming 30% gas density reducition (for a 25 μA beam) on 10 atmospheres of gas.

Targets were stringently cleaned prior to these studies by repetitively exposing their inner surfaces to gas mixtures of 5% O_2 in neon (10 atm.) during proton irradiations. Cumulative doses of 25 μA hr were sufficient to reduce surface bound carbon to low steady-state levels. However, surface bound carbon increased upon re-exposure to target N_2.

RESULTS AND DISCUSSION: Table 1 lists target volumes, exposed surface areas, and measured carrier CO_2 levels from three experiments. In each experiment, 25 μA of beam was placed on target for 15 minutes. The same 16.5 miL thick aluminum window was used in each instance yielding 13.4 MeV of proton energy on gas. The carrier CO_2 measurement was categorized according to the target gas contribution and other sources. The gas contribution was calculated from target pressure and volume data, and our previous measurements of total carbon content within the target gas. We assumed that all carbonaceous material within the gas was combusted to CO_2 under these circumstances.

TABLE 1
CORRELATION OF TARGET SURFACE AREA WITH CARRIER CO_2 OUTPUT

Target	Surface	Carrier CO_2 Output (nmol)	
Volume (cm^3)	Area (cm^2)	Gas Contribution	Other Sources
212	255	24	38
94	127	12	20
68	102	8	15

Results from these studies suggest that a correlation exists between target surface exposed to beam and carrier contributions arising from sources other than the target gas. Based on our earlier observations made by EID spectroscopy, we must assume that these other sources arise from the release of surface bound carbon from the oxide overlayer when irradiated.

STUDIES ON THE EFFECT OF WINDOW DEFORMATION ON THE SCATTERING AND ENERGY PROFILES OF THE BEAM: POTENTIAL EFFECTS CONTRIBUTING TO TARGET MASS

Recently, we installed a preformed 18.5 miL thick aluminum window, possessing a 5 mm hemispherical deformation, onto our 77 mL volume conical target, but with the deformation placed concave into the target. We did this because pressure and beam induced deformation of our flat aluminum windows would cause them to bow outward beyond the helium cooling axis, which eventually resulted in window failure. We thought that placing a preformed window in a concave geometry would provide additional radial strength to minimize further deformation, and also optimum window cooling thus increasing window lifetime.

The windows were fabricated from 6061 aluminum alloy. The alloy exists in a T_6 state of hardness (the highest level), but can be converted to a T_0 workable state through heating of the alloy for several hours at 500°C. Once in this state, the windows can be deformed over a mandrel with little or no stress added to the surface structure. The alloy automatically reverts back to its original state of hardness over a 48 hour period.

In-direct observations made on [^{11}C]cocaine specific activity suggested that target mass contributions were somewhat reduced with the window placed in a concave configuration. We have yet to verify this directly through CO_2 target mass measurements. Even so, this peaked our interest in what effect window geometry might have on the scattering and energy profiles of the proton beam. These aspects could have significant effects on target surface contributions to mass.

EXPERIMENTAL PROCEDURE: In the beam scattering profile study, we used an optical target fabricated from quartz in the same shape and size as our conical production target. The preformed aluminum windows were sealed onto the front-end of the optical target both in the concave and convex configuration. In both instances, the target was filled to 1 atmosphere with neon gas, and irradiated with a 18 MeV proton beam focussed to a 10 mm spot size. Data was acquired with color video camera interfaced with a digital frame grabber board on a PC computer. This

allowed us to collect and overlay beam scattering profiles for the two window geometries.

In the beam energy profile studies, nickel foils (5 cm o.d. x 1 miL thick) were mounted in a test chamber 10 cm behind the beam entry window. This distance was identical to our conical target length. The chamber was filled with 1 atmosphere of helium gas, so gas induced alteration of the beam energy profile could be ignored. The front preformed window was mounted both concave and convex to the nickel foils, and short irradiations were carried out using the same conditions described above. After bombardment, the foils were removed, and cut into 3 mm wide rings for analysis by gamma spectroscopy. Each ring was assessed for relative distributions of ^{55}Co and ^{57}Co activities which were formed from the $^{58}Ni(p,\alpha)^{55}Co$ and $^{60}Ni(p,\alpha)^{57}Co$ reactions, respectively. Corrections were made to the data for relative abundances of the nickel isotopes, and for detection effiency of the gamma energies (931 KeV and 122 Kev, respectively) used to measure the cobalt abundances.

Since the proton reactions on nickel exhibit significantly different dependences on energy below 13.5 MeV, this method provides a excellent diagnostic tool for looking at beam energy profile (Kaufman, 1960). Figure 5 illustrates this feature in a correlation of proton energy with the isotope cross section ratio.

RESULTS AND DISCUSSION: Results from the beam scattering studies in the optical target showed no significant differences in beam profile for the two window geometries.

Figures 6 and 7 illustrate the variation of the beam energy, depicted by the ^{55}Co-to-^{57}Co ratio, as a function of the radial distance from the center axis of the beam, for target windows mounted concave and convex to the target, respectively. The striking feature here is that the beam energy profile is significantly affected by window geometry. We observed much higher beam energies incident on the outer fringes of the nickel foil, when the front target window was mounted concave to the target, than when the window was mounted convex.

One might rationalize that with a higher energy beam incident on the target surface, the Bragg peak would occur deeper within the material and thus have less of an effect on surface release of carbonaceous material entrained within the outer oxide layer. This aspect certainly bears further investigation.

SUMMARY

Clearly, the above studies demonstrate that the $[^{11}C]O_2$ specific activity will benefit enormously from targets whose size and shape will

minimize surface exposure to beam. It goes without saying that smaller volume targets will also minimize gas contributions to mass. In addition, attention to window geometry may have beneficial affects on target surface contributions to mass. Of course, one can only capitalize on this feature if sufficient beam energy is available to expend on a thick window.

Unfortunately, there are practical considerations when trying to achieve high specific activity $[^{11}C]O_2$. We have observed (see Figure 8) that as the amount of carrier mass generated within the target is minimized, the extraction efficiency of carbon-11 activity as $[^{11}C]O_2$ decreases from theoretical expectations. This phenomenon appears to occur independent of the nature of the material used to fabricate the target (we have compared identical volume cylindrical targets fabricated from aluminum and nickel), and independent of the size and shape of the target (we have compared cylindrical targets of various volumes with our standard 77 mL conical target). For a lack of a better term, we refer to this phenomenon as a carrier effect. Ultimately, one is faced with the prospect of compromising between $[^{11}C]O_2$ specific activity, and the amount of $[^{11}C]O_2$ that can be extracted from the target after a reasonable irradiation time.

ACKNOWLEDGEMENT: This research was carried out at Brookhaven National Laboratory under contract DE-ACO2-76CH00016 with the U. S. Department of Energy and supported by its Office of Health and Environmental Research. Research was also supported by the National Institutes of Health under Grant NS-15380.

REFERENCES

Burns H.D., Dannals R.F., Langstrom B., Ravert H.T., Zemyan S.E. Duelfer T., Wong D.F., Frost J.J., Kuhar M.J. and Wagner H.N. (1984) (3-N-[^{11}C]methyl)spiperone, a ligand binding to dopamine receptors: Radiochemical synthesis and biodistribution studies in mice. *J. Nucl. Med.* **25**, 1222.

Czanderna A.W. (ed.) (1975) Methods of Surface Analysis, *Elsevier Scientific Publishing*, New York.

Dewey S.L., MacGregor R.R., Brodie J.D., Bendriem B., King P.T., Volkow N.D., Schlyer D.J., Fowler J.S., Wolf A.P. Gatley J. and Hitzemann R. (1990) Mapping muscarinii receptor in human and baboon brain using [N-^{11}C-methyl]- benztropine. *Synapse* **5**, 213.

Farde L., Hall H., Ehrin E. and Sedvall G. (1986) Quantitative analysis of D2 dopamine receptor binding in the living human brain by PET. *Science* **231**, 258.

Goekeler U.K. (1989) Determination of oxygenated hydrocarbons in fuel with oxygen selective detector. *Am. Lab.*, June, 34.

Hatano K., Ishiwata K., Kawashima K., Hatazaw J., Itoh M. and Ido T. (1989) D2-dopamine receptor specific brain uptake of carbon-11-labeled YM-09151-2. *J. Nucl. Med.* **30**, 515.

Iwata R., Hatano K., Yanai K. Takahashi T., Ishiwata K. and Ido T. (1991) A semi-automated synthesis system for routine preparation of [^{11}C]YM-09151-2 and [^{11}C]pyrilamine from [^{11}C]methyl iodide. *Appl. Radiat. Isot.* **42**, 202.

Kaufman S. Reactions of protons with ^{58}Ni and ^{60}Ni (1960) *Phys. Rev.* **117**, 1532.

Langstrom B. and Lundqvist H. (1976) The preparation of carbon-11 labeled methyl iodide and its use in the synthesis of carbon-11 labeled methyl-L-methionine. *Int. J. Appl. Radiat. Isot.* **27(7)**, 357.

Pascali C., Pike V.W. and Turton D.R. (1990) The radiosynthesis of NCA [O-methyl-^{11}C]viqualine through an N-trityl-protected intermediate, as a potencial PET radioligand for 5HT re-uptake sites. *J. Label. Compd. Radiopharm.* **28**, 1341.

Suzuki K., Inoue O., Hashimoto K., Yamasaki T., Kikuchi M. and Tamate K. (1985) Computer-controlled large scale production of high specific activity [^{11}C]RO 15-1788 for PET studies of benzodiazepine receptors *Int. J. Appl. Radiat. Isot.* **36**, 971.

Watkins G.L., Jewett D.M., Mulholland K., Kilbourne M.R. and Toorongian S.A. (1988) a captive solvent method for rapid N-[^{11}C]methylation of secondary amines: Application to the benzodiazepine, 4'-chlorodiazepam(RO5-4864). *Appl. Radiat. Isot.* **39**, 441.

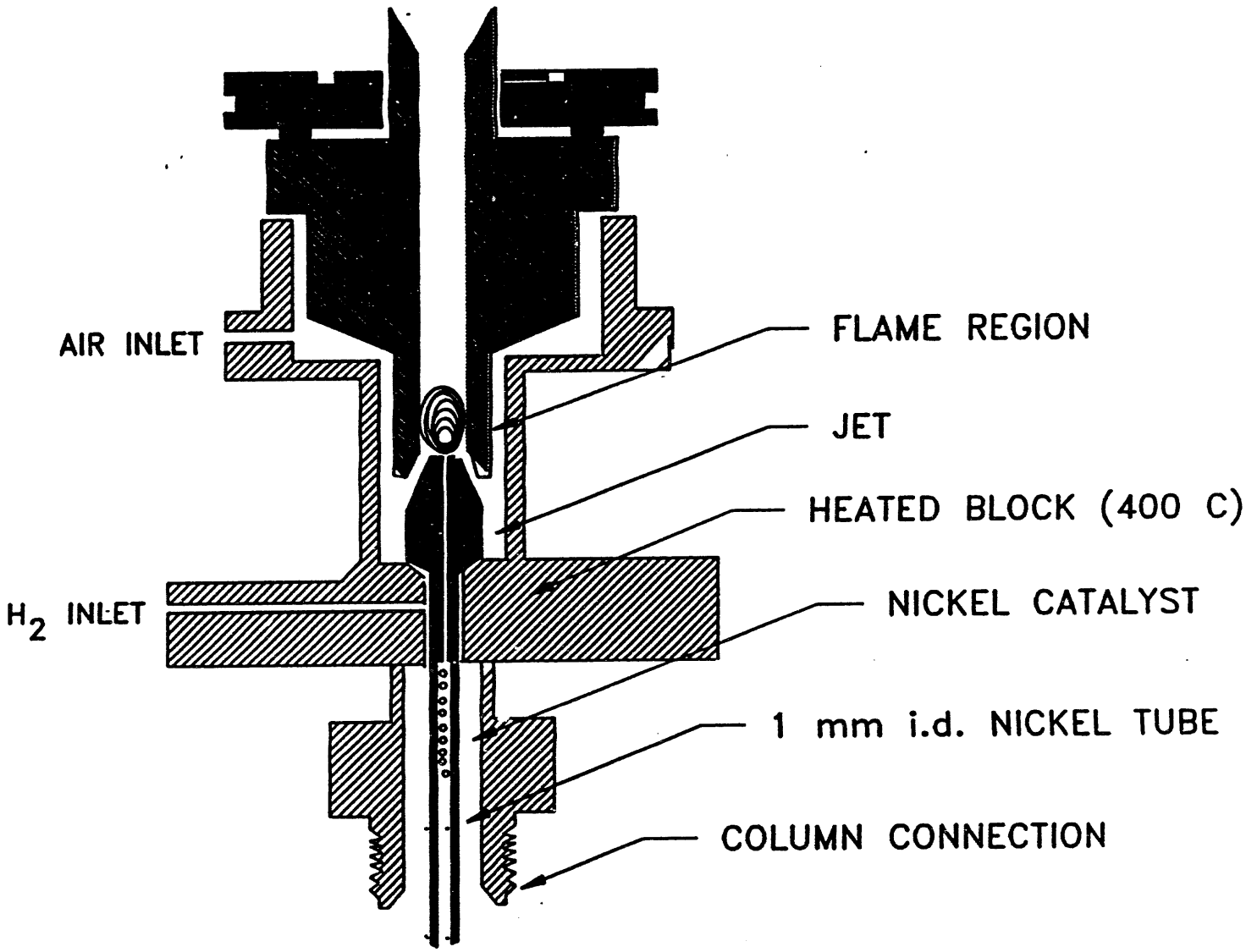

Figure 1 Modified flame ionization detector from a Hewlett Packard 5890A gas chromatograph used for carbon oxide analysis.

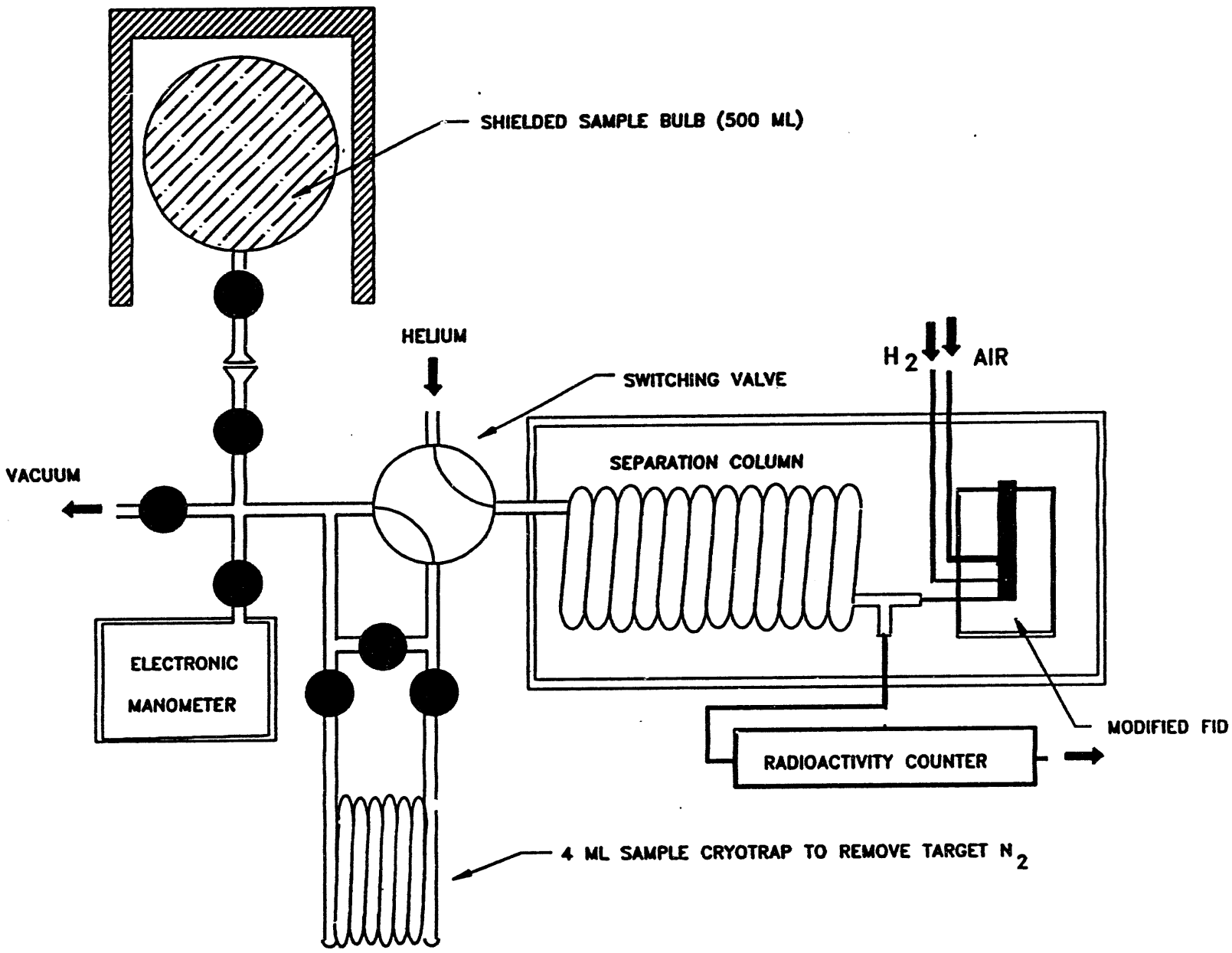

Figure 2 Gas sampling port and gas chromatograph for carbon oxide analysis.

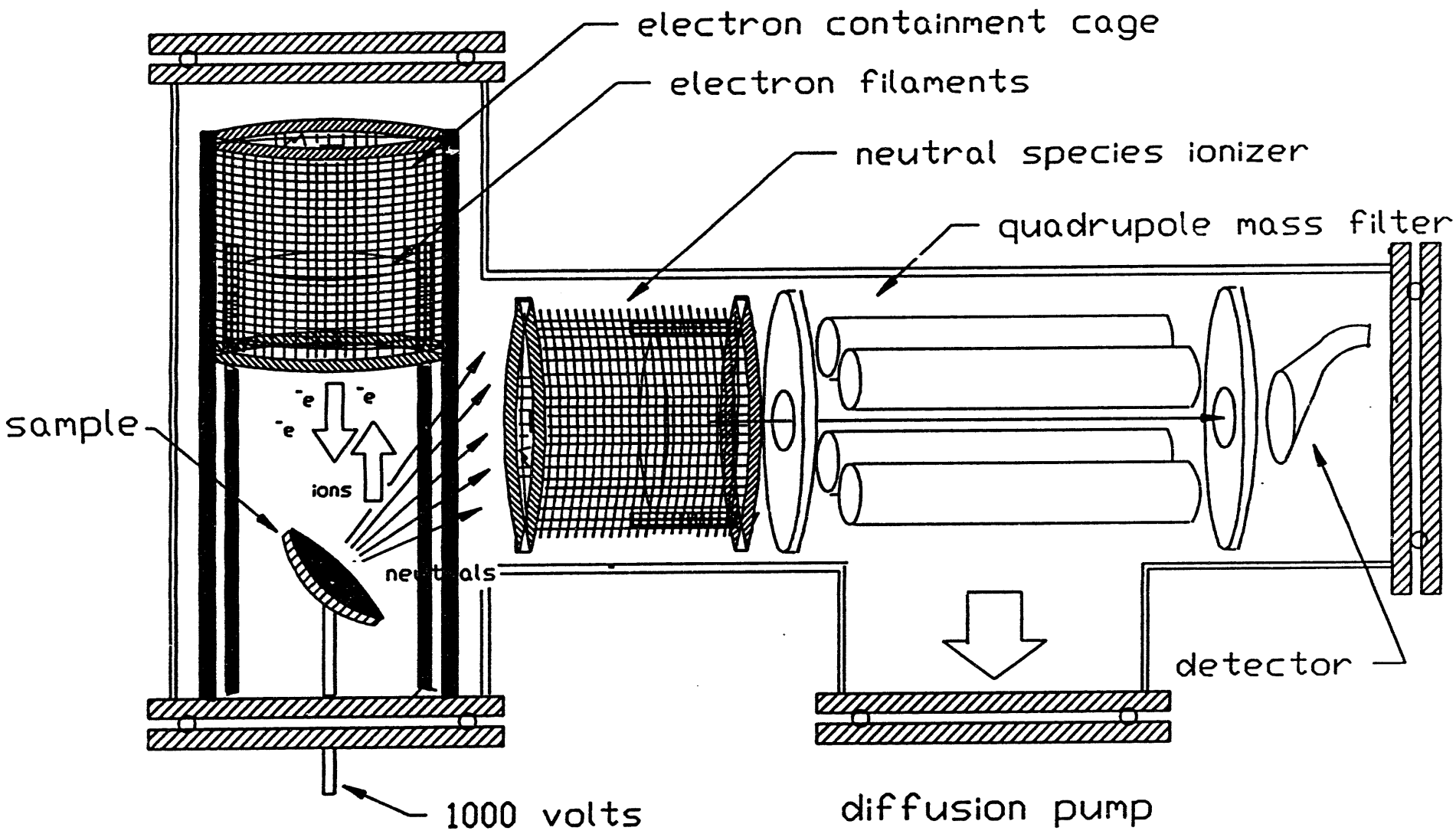

Figure 3. Electron induced desorption instrument used for surface analysis

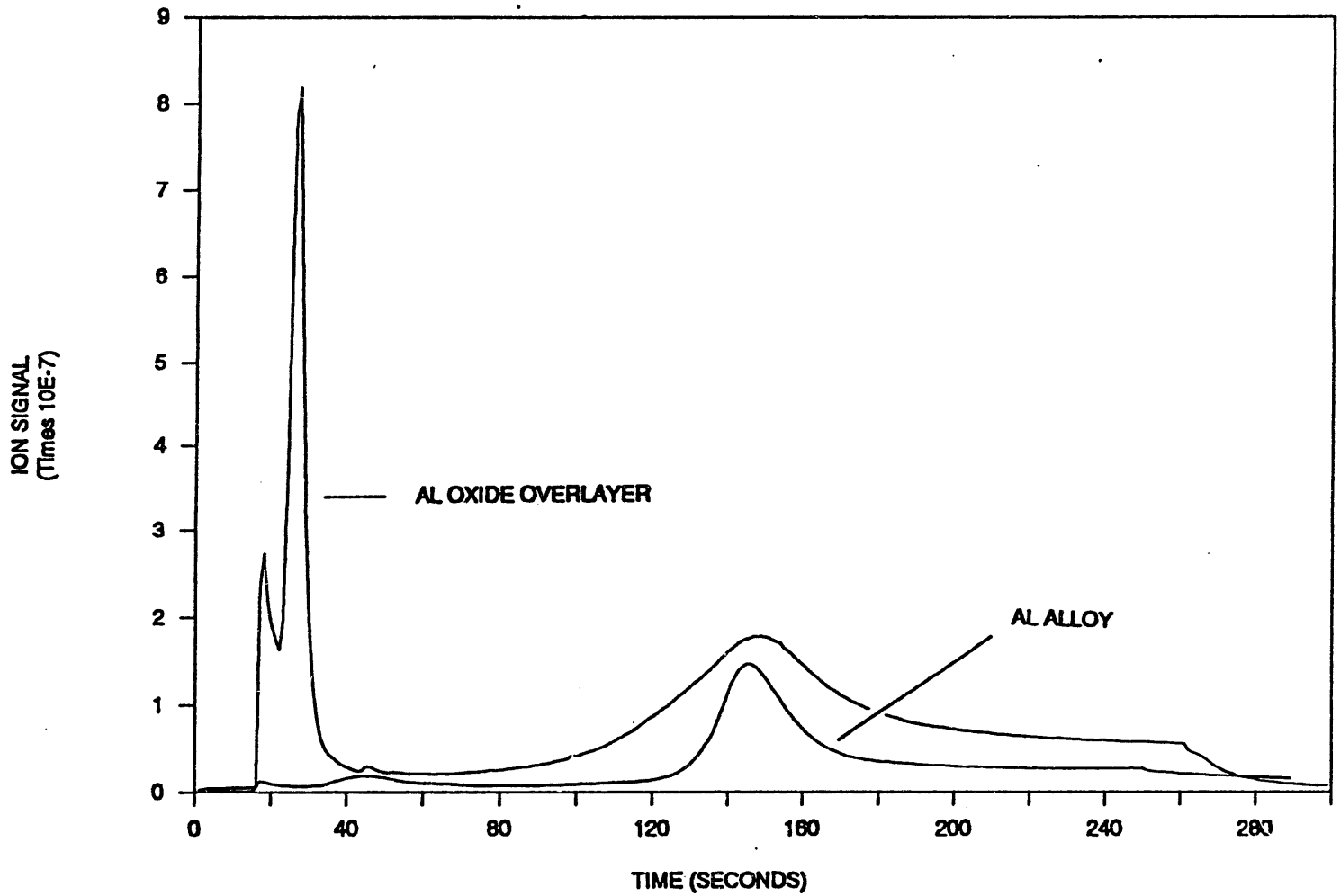

Figure 4 Electron induced desorption spectrum (at 1000 volt electron acceleration) of CO_2 (m/z 44) from a clean 6061 aluminum alloy surface, and from a treated 6061 alloy surface that possessed a 10^4 monolayer thick coating of oxide, and was exposed to 10 ppm levels of CO_2 in N_2 gas.

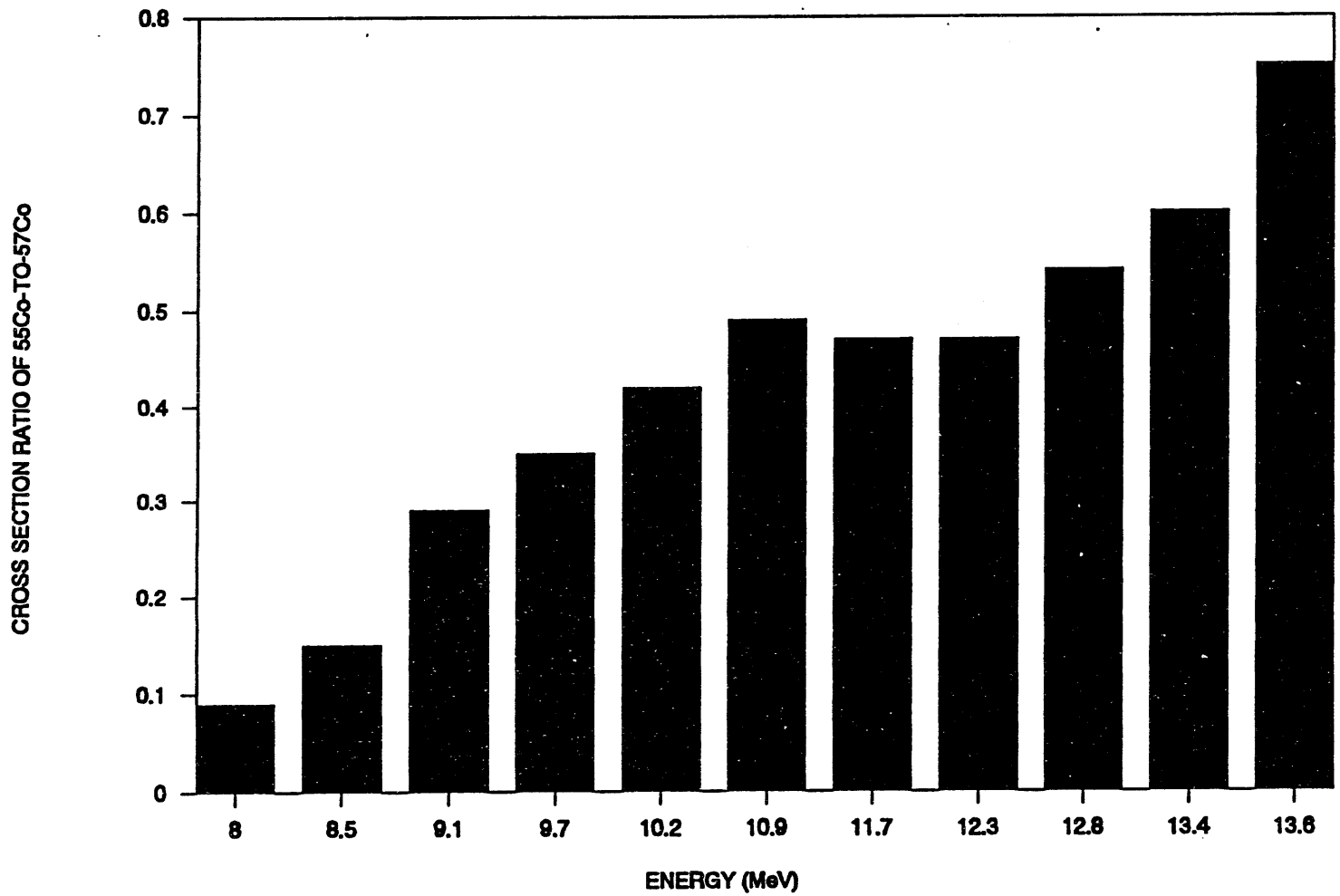

Figure 5 Energy correlation diagram of $^{58}Ni(p,\alpha)^{55}Co$ and $^{60}Ni(p,\alpha)^{57}Co$ cross section ratios.

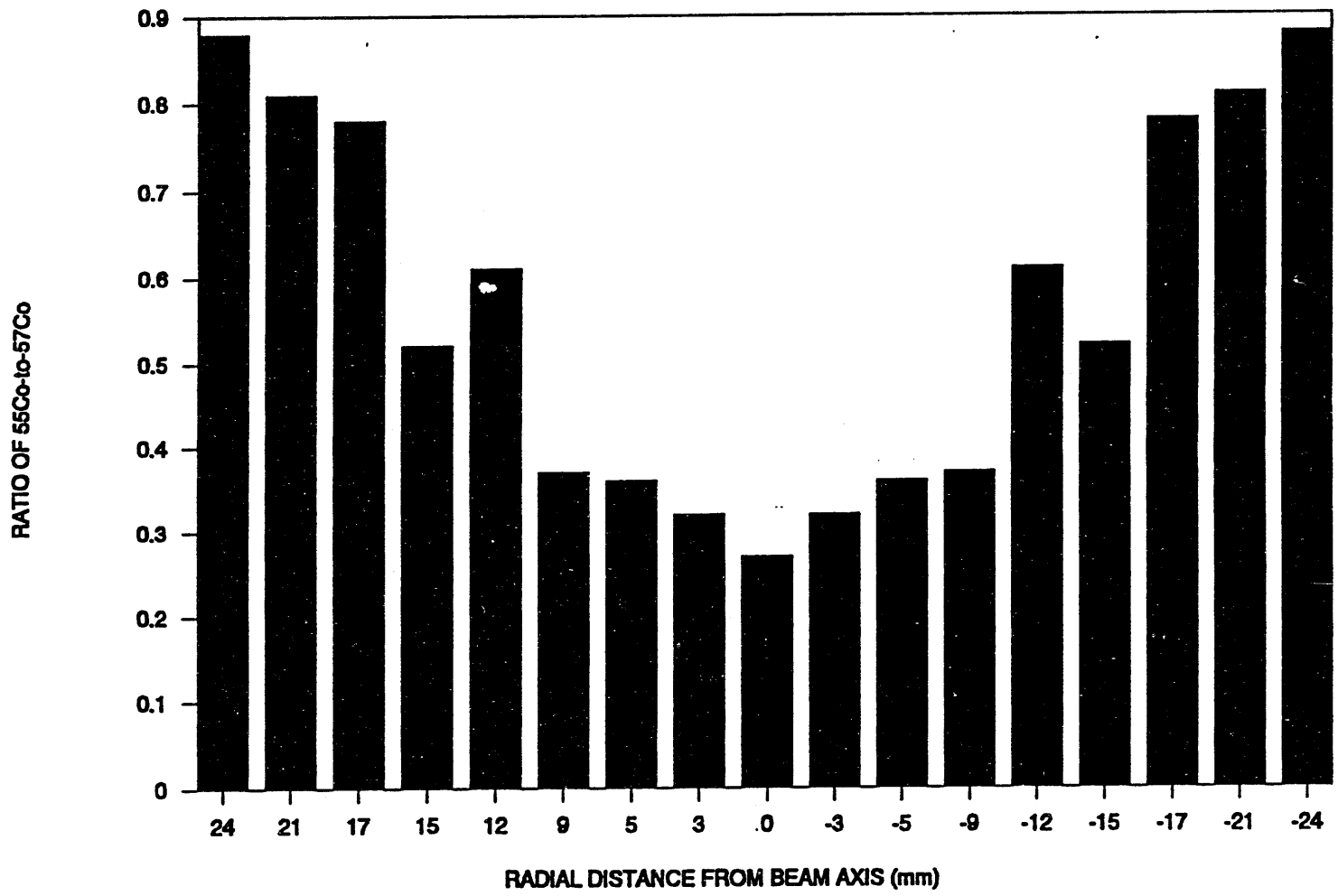

Figure 6 Variation in the proton beam energy, depicted by the ^{55}Co-to-^{57}Co ratio, as a function of the radial distance from the center axis of the beam, for a concave mounted target window.

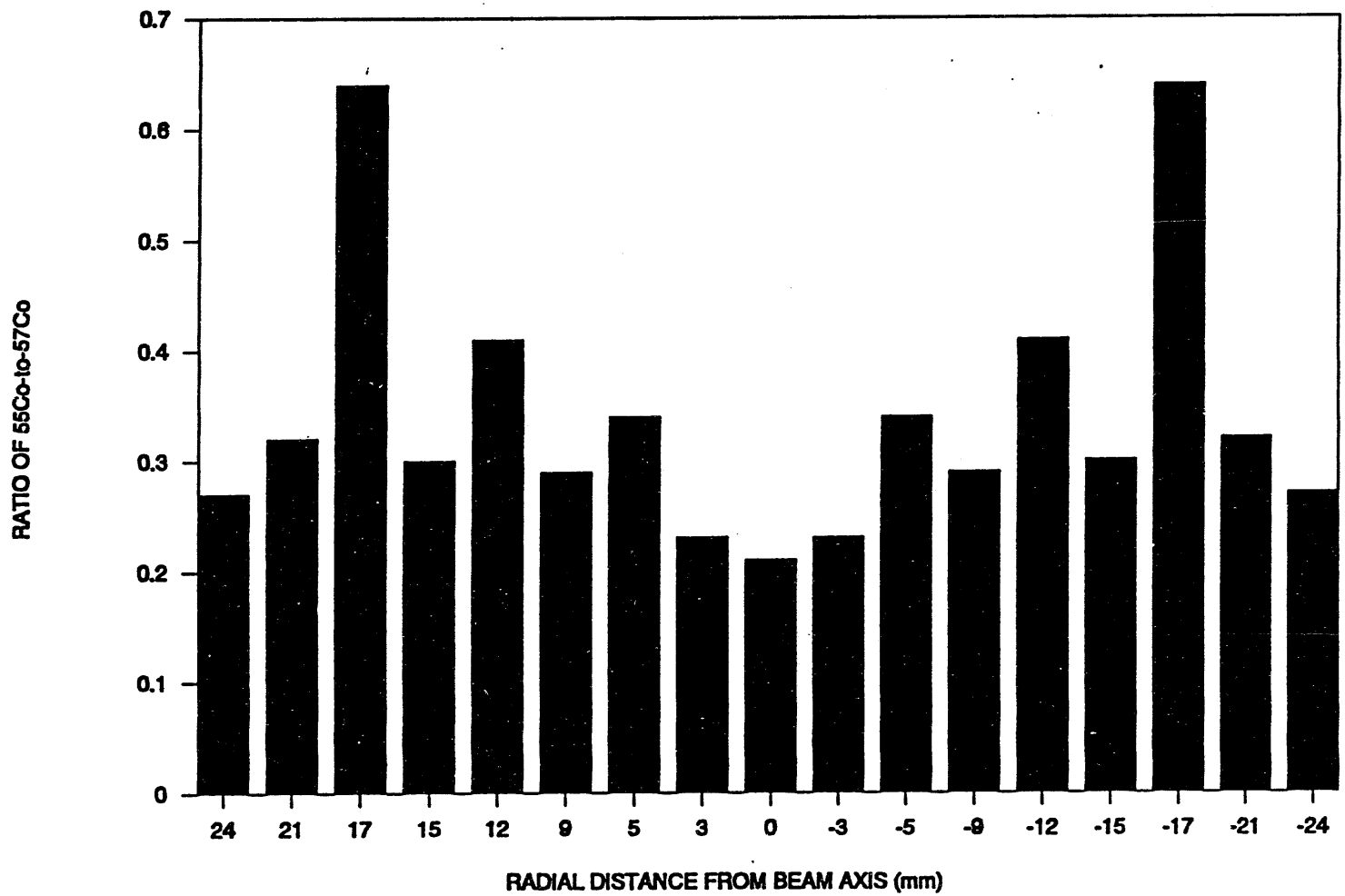

Figure 7 Variation in the proton beam energy, depicted by the ^{55}Co-to-^{57}Co ratio, as a function of the radial distance from the center axis of the beam, for a convex mounted target window.

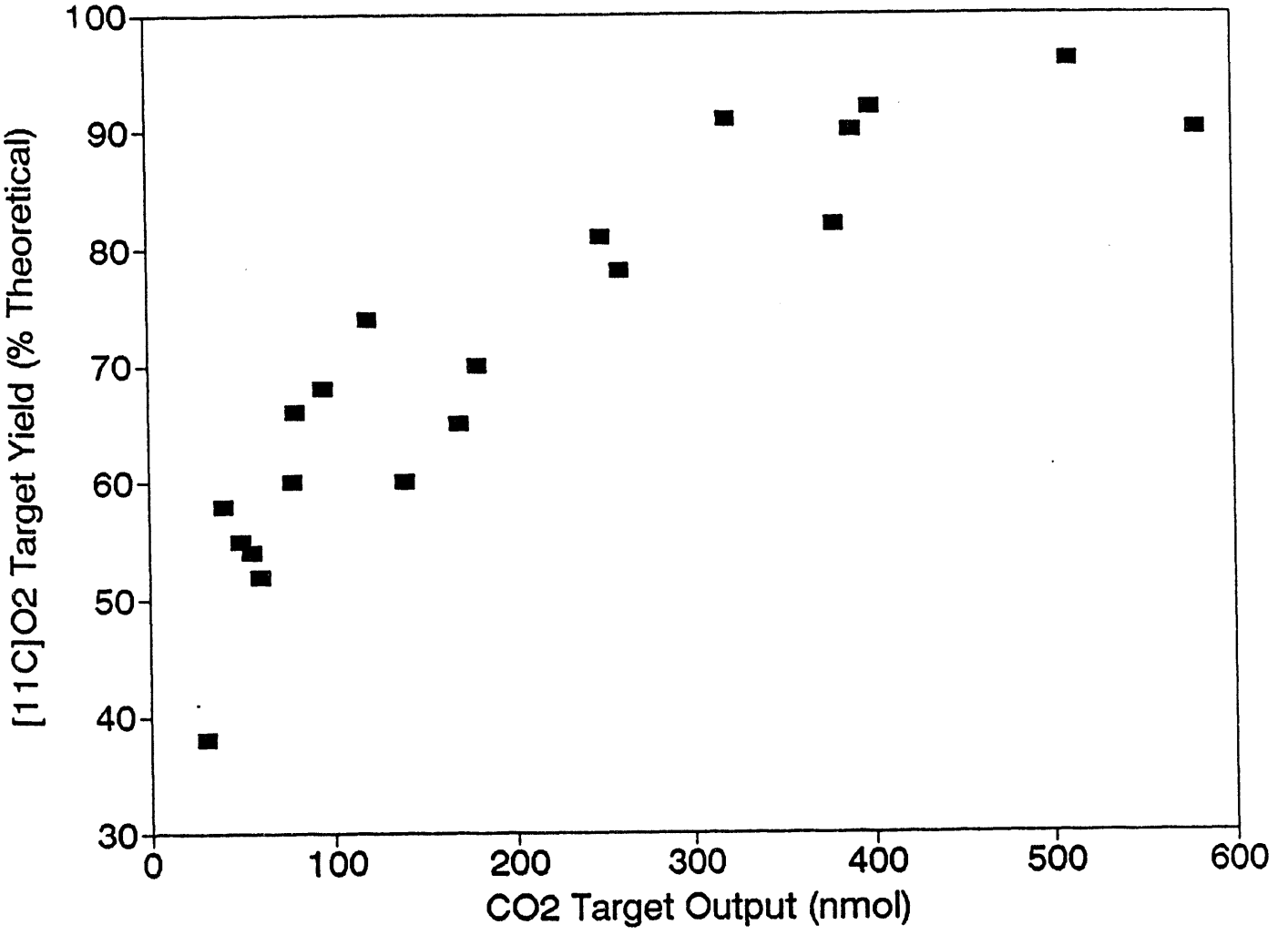

Figure 8. Correlation between target output of carrier CO_2 and the extracted target yield of $[^{11}C]O_2$.

DATE
FILMED
6/14/94

END